A Mathematical Framework for Analysis of Water Tracers. Part II: Understanding Large-Scale Perturbations in the Hydrological Cycle due to CO_2 Doubling

HANSI K. A. SINGH AND CECILIA M. BITZ

Department of Atmospheric Sciences, University of Washington, Seattle, Washington

AARON DONOHOE

Applied Physics Laboratory, University of Washington, Seattle, Washington

JESSE NUSBAUMER

Department of Atmospheric and Oceanic Sciences and Cooperative Institute for Research in Environmental Science, University of Colorado Boulder, Boulder, Colorado

DAVID C. NOONE

Department of Earth, Ocean, and Atmospheric Sciences, Oregon State University, Corvallis, Oregon

(Manuscript received 8 April 2016, in final form 16 June 2016)

ABSTRACT

The aerial hydrological cycle response to CO_2 doubling from a Lagrangian, rather than Eulerian, perspective is evaluated using information from numerical water tracers implemented in a global climate model. While increased surface evaporation (both local and remote) increases precipitation globally, changes in transport are necessary to create a spatial pattern where precipitation decreases in the subtropics and increases substantially at the equator. Overall, changes in the convergence of remotely evaporated moisture are more important to the overall precipitation change than changes in the amount of locally evaporated moisture that precipitates in situ. It is found that CO_2 doubling increases the fraction of locally evaporated moisture that is exported, enhances moisture exchange between ocean basins, and shifts moisture convergence within a given basin toward greater distances between moisture source (evaporation) and sink (precipitation) regions. These changes can be understood in terms of the increased residence time of water in the atmosphere with CO_2 doubling, which corresponds to an increase in the advective length scale of moisture transport. As a result, the distance between where moisture evaporates and where it precipitates increases. Analyses of several heuristic models further support this finding.

1. Introduction

In this study, we present new insights on large-scale perturbations to the aerial hydrological cycle due to quasi-equilibrium CO_2 doubling by employing a novel Lagrangian framework that exploits data from numerical water tracers (WTs) implemented in a global climate model (GCM). This framework offers an alternative perspective to existing theories of hydrological cycle change, which are primarily Eulerian and focus on the local energetic (i.e., radiative and diabatic) and dynamic (moisture flux convergence) processes that drive hydrological cycle perturbations. We begin by reviewing evidence for changes in the hydrological cycle due to CO_2-induced warming and discuss how these changes are understood using Eulerian theoretical frameworks. We then consider in depth how our Lagrangian framework, utilizing WTs, offers a complementary lens for viewing perturbations to the hydrological cycle due to CO_2 doubling.

The hydrological cycle is, undoubtedly, of great importance to human societies and natural ecosystems. Several lines of observational evidence suggest that the hydrological cycle has shifted relative to its preindustrial state in response to anthropogenic perturbations. Ocean

Corresponding author address: Hansi Singh, Department of Atmospheric Sciences, University of Washington, Box 351640, Seattle, WA 98195.
E-mail: hansi@atmos.washington.edu

DOI: 10.1175/JCLI-D-16-0293.1

salinities appear to be trending upward in the tropics and downward in the high latitudes, suggesting that the climatological difference between evaporation and precipitation has increased and the hydrological cycle has intensified (Helm et al. 2010; Durack et al. 2012). Surface specific humidity has increased in response to increased surface temperatures (Willett et al. 2007), and terrestrial precipitation over the NH subtropics has declined (Zhang et al. 2007).

GCM studies predict a medley of further hydrologic changes with planetary warming. In the tropics, models predict enhanced precipitation seasonality (Chou et al. 2007) and more heavy precipitation events (Meehl et al. 2005; Hu et al. 2012; Lau et al. 2013). The subtropics are expected to dry (Allan et al. 2010) and widen (Seager et al. 2007; Seidel et al. 2008). The midlatitude storm tracks are expected to shift poleward (Hall et al. 1994; Yin 2005; Bengtsson et al. 2006; Chang et al. 2012) and change in intensity (O'Gorman 2010; Chang et al. 2012), the characteristic length scale of atmospheric eddies is expected to increase (Kidston et al. 2010; Rivière 2011), and moisture transport into the polar regions is expected to increase (Hwang and Frierson 2010). In the high latitudes, precipitable water is projected to increase (Serreze et al. 2012) and the hydrological cycle to intensify (Bengtsson et al. 2011). As land areas become more arid (Dai 2012; Sherwood and Fu 2014), the relative importance of oceanic moisture sources for continental precipitation is expected to increase (Gimeno et al. 2013).

From a global perspective, there are two important principles that govern how the hydrological cycle responds to anthropogenic greenhouse gas emissions. First, tropospheric water vapor increases at a rate dictated by the Clausius–Clapeyron (C-C) equation, a 7% increase in specific humidity per °C of warming (Manabe and Wetherald 1975; Held and Soden 2006). Second, precipitation and evaporation cannot increase at the C-C rate because of energetic constraints. In particular, evaporation is limited by the surface energy budget, while precipitation is limited by the atmospheric longwave radiative cooling rate and the dry static energy (DSE) flux divergence. As a result, both precipitation and evaporation increase with temperature at a slower rate, 1% to 3% per °C of warming, which varies depending on the GCM and emissions scenario (Mitchell et al. 1987; Stephens et al. 1994; Allen and Ingram 2002).

An influential study attributing changes in the hydrological cycle to C-C scaling of atmospheric moisture with temperature is that of Held and Soden (2006). While neither P nor E scales at the C-C rate, Held and Soden (2006) showed that the change in $P - E$ scales with the change in temperature at the C-C rate. If relative humidity (RH) stays constant and atmospheric motions are unchanged, then the atmospheric moisture flux convergence, equivalent to $P - E$, scales at the C-C rate, amplifying the mean state $E - P$ cycle and transporting more moisture poleward. As a result, areas where P exceeds E in the climatology will get wetter, while areas where E exceeds P will dry.

Nevertheless, perturbations to the atmospheric moisture divergence, $\nabla \cdot Q$, which are responsible for the change in $P - E$, are not solely due to increased atmospheric moisture. Indeed, many studies that have followed Held and Soden (2006) have qualified the results presented therein, particularly in regard to the importance of dynamic (rather than thermodynamic) drivers of hydrological cycle changes seen in GCMs (see, e.g., Seager et al. 2010).

Others argue that closer inspection of the spatial pattern of precipitation change reveals inconsistencies with the thermodynamic argument of Held and Soden (2006). Scheff and Frierson (2012b) and Scheff and Frierson (2012a) point out that precipitation does not decrease uniformly within the subtropics in CMIP5 models; instead, the subtropics dry preferentially on their poleward flanks as the subtropical dry zones expand, suggesting that this and the accompanying poleward shift of the storm tracks and jet are a dynamic response to CO_2-induced warming. Corresponding changes in precipitation are not a simple result of increased atmospheric moisture, but are rather due to poleward shifts in general circulation features that are common to most GCM predictions and that are not easily explained by a single, unifying theory (see, e.g., Vallis et al. 2014; Lorenz 2014).

Moreover, increases in E and P are limited energetically well below the C-C rate. The latent energy associated with precipitation is a source of heating, and precipitation is limited by the rate at which the atmosphere dissipates this excess energy radiatively (Mitchell et al. 1987; Stephens and Ellis 2008; Pendergrass and Hartmann 2014) and dynamically (Muller and O'Gorman 2011). The surface energy budget also constrains evaporation below the C-C rate. Increased relative humidity, increased static stability at the surface, decreased wind speed, and increased cloud albedo all act to constrain evaporation increases well below the C-C rate (Boer 1993; Richter and Xie 2008; Lorenz et al. 2010).

In this study, we use numerical WTs implemented in a state-of-the-art GCM to present a Lagrangian schema of hydrological cycle change complementary to existing paradigms, namely C-C scaling of moisture and energetic constraints on E or P. So far, only one other study has used numerical WTs to study changes in the aerial

hydrological cycle caused by increased CO_2: Bosilovich et al. (2005) showed that the cycling rate of water in the atmosphere decreased, and the residence time scale increased. Such changes have also been predicted by other studies, which have shown that increasing atmospheric moisture at a higher rate than evaporation or precipitation requires that atmospheric moisture residence times must increase (see Trenberth 1998; Held and Soden 2006; van der Ent and Savenije 2011). Here, we also examine the implications of this increased atmospheric moisture residence time.

We find that, from a Lagrangian perspective, the changes in precipitation due to changes in evaporation (local and remote) are uniformly positive and have little latitudinal structure, while changes in precipitation due to changes in transport contain much of the spatial structure of the total precipitation change. Furthermore, we find that changes in the local contribution to the precipitation are small, while changes in the remote contribution are much larger. We show that many of these changes can be understood in terms of a decreasing moisture depletion tendency, which decreases precipitation efficiency (thereby decreasing the tendency of atmospheric moisture to precipitate) and increases the atmospheric moisture residence time and the moisture transport length scale, the distance between moisture source and sink regions.

This paper is structured as follows. In section 2, we review the mathematical development presented in Part I and introduce notation for applying it to perturbation studies. In section 3, we describe the setup of our GCM WT experiments, and in section 4, we analyze the results of these experiments using the mathematics developed earlier. In section 6, we analyze several heuristic models of atmospheric moisture transport to support the results of our GCM experiments. We discuss our results, consider further implications of our work, and offer some concluding remarks in section 7.

2. Overview of mathematical framework and perturbation methods

In Part I of this paper (Singh et al. 2016a, hereafter Part I), we developed a linear algebra framework for analyzing the output from experiments employing numerical WTs. We review this framework here, and introduce some additional notation for analyzing perturbations to the mean state, which we will use in our study of the hydrological cycle response to CO_2 doubling.

In general, the precipitation P_i in a tagged region is due to the local evaporation E_i, reduced by the divergence of locally evaporated moisture from the tagged region and augmented by the convergence of remotely evaporated moisture from all other tagged regions (denoted E_j) such that tagged regions cover the entire globe:

$$P_i = E_i - e_i E_i + \sum_{i \neq j} e_j f_{ji} E_j, \tag{1}$$

where e_i is the fraction of moisture evaporated in the ith region that precipitates elsewhere (and is, therefore, not available to precipitate locally), e_j is the fraction of moisture evaporated in the jth region that precipitates outside the jth region, and f_{ji} is the fraction of total moisture exported from region j that falls in region i. Thus, the product $e_j f_{ji} E_j$ represents the fraction of E_j (the total moisture evaporated from region j) that is exported from the jth region and subsequently precipitates in the ith region. Summing the contributions from all regions j to region i gives the total amount of remotely evaporated moisture that converges into region i.

In matrix form, we can write Eq. (1) compactly as

$$\mathbf{P} = \mathbf{E} - \mathbf{TE} + \mathbf{FTE}, \tag{2}$$

where $\mathbf{T}$ is a diagonal matrix whose entries e_j represent the fraction of moisture evaporated from region j that precipitates outside region j; and $\mathbf{F}$ is a hollow matrix (diagonal entries are zero) whose i, j-th entry is equal to f_{ji}, the fraction of the exported moisture evaporated from the jth region that precipitates in the ith region. By definition, the diagonal entries of $\mathbf{F}$ must be nil (i.e., $f_{ii} = 0$), since any moisture that both evaporates and precipitates in region i is accounted for in the $E_i - e_i E_i$ term, which is the contribution of locally evaporated moisture to the local precipitation. In brief, Eq. (2) states that $\mathbf{P}$ is composed of contributions from the local evaporation ($\mathbf{E}$), decreased by the amount of this local evaporation that diverges ($\mathbf{TE}$), and increased by the amount of remote evaporation that converges ($\mathbf{FTE}$).

We may also write Eq. (2) more compactly as

$$\mathbf{P} = \mathbf{ME}, \tag{3}$$

where the operator $\mathbf{M}$ is defined as

$$\mathbf{M} = \mathbf{I} - \mathbf{T} + \mathbf{FT}. \tag{4}$$

In the ensuing perturbation analysis, we will decompose Eq. (2) into mean state and perturbation quantities to compute how changes in the local evaporation, the divergence of locally evaporated moisture, and the convergence of remotely evaporated moisture all contribute to changes in the precipitation. In terms of notation, we will use the Δ operator to denote a difference between the CO_2-doubling experiment and the control, that is, $\Delta X = X_{2\times CO_2} - X_{\text{control}}$, where X is either a vector quantity (such as $\mathbf{P}$ or $\mathbf{E}$) or a matrix

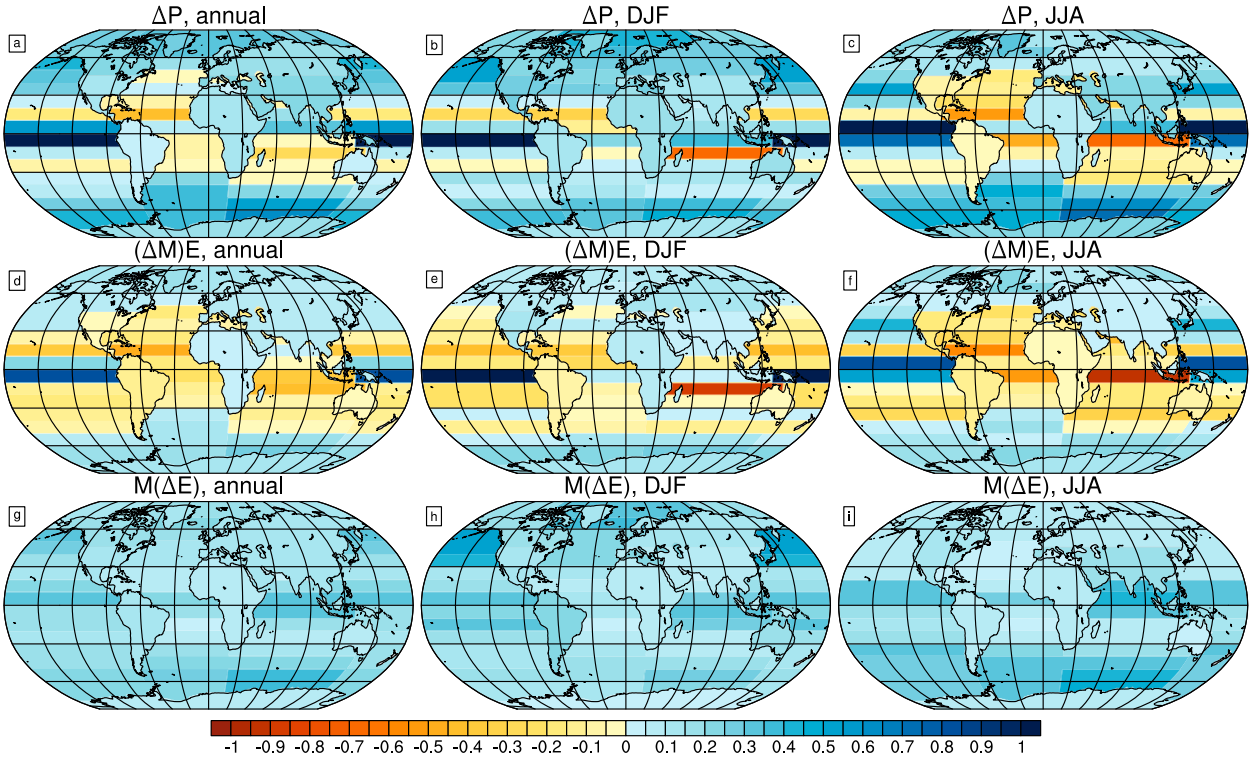

FIG. 1. Perturbation analysis of the contribution of $\Delta\mathbf{M}$ and $\Delta\mathbf{E}$ to the change in precipitation with CO_2 doubling: (a)–(c) the change in precipitation; (d)–(f) the change in precipitation due to changes in the transport operator **M**; and (g)–(i) the change in precipitation due to changes in evaporation, **E**. Each of these quantities is shown (left) in the annual average, (middle) averaged over DJF, and (right) averaged over JJA, and all are in units of mm day^{-1}.

(such as **T** or **F**). In our perturbation analysis, we will also assume that perturbed quantities can be decomposed linearly, in that for a given product XY, we can write the perturbation decomposition as $\Delta(XY) \approx (\Delta X)Y + X(\Delta Y)$, and the nonlinear term $(\Delta X)(\Delta Y)$. In all the following analyses, we have found that the nonlinear terms are very small (<5% of the total perturbation), and have neglected them.

3. Model experiments

The control experiment (piC, for preindustrial control), as described in Part I, was run using the fully coupled Community Earth System Model 1.0 (CESM1) with all model components at 1° spatial resolution and with all model parameters set at preindustrial levels. Aerial water was tagged with its region of origin in 10° latitude bands over each ocean basin. Each continent was tagged separately, with Eurasia and North America subdivided into two parts each. There are 49 distinct tagged regions in total, encompassing the entire globe.

For Part II, a second experiment was branched from the preindustrial control simulation in which atmospheric CO_2 was doubled from its preindustrial concentration of approximately 290 ppm to 580 ppm. All other atmospheric variables, including concentrations of trace gases, aerosol forcing, and total solar irradiance, were held at preindustrial levels. The simulation was allowed to run without WTs for 270 years to approach a quasi-equilibrium state. For a final 30 years, WTs with the same spatial configuration as for piC were introduced. We refer to the final 30 years of this run, years 270 to 300, as the equilibrium CO_2-doubling experiment (Eqm2×CO_2). The net TOA energetic imbalance in Eqm2×CO_2 is less than 0.1 W m^{-2}. Climatologies are created from 30 years of model output with WTs. All perturbation quantities are given as the difference between the CO_2-doubling experiment and the control, Eqm2×CO_2–piC.

4. Aerial hydrological cycle perturbations resulting from evaporation changes versus transport changes

a. *Decomposing the change in* **P**

The total change in the precipitation in Eqm2×CO_2 (Figs. 1a–c) can be decomposed as

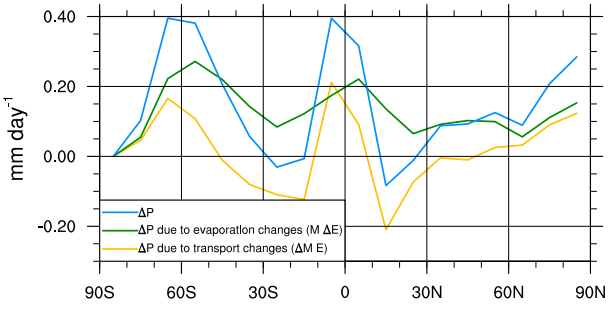

FIG. 2. The change in precipitation, $\Delta\mathbf{P}$, due to changes in transport, $(\Delta\mathbf{M})\mathbf{E}$, and changes in evaporation, $\mathbf{M}(\Delta\mathbf{E})$. All quantities are annually averaged zonal means (averaged over the ocean domain only), and shown in units of mm day^{-1}.

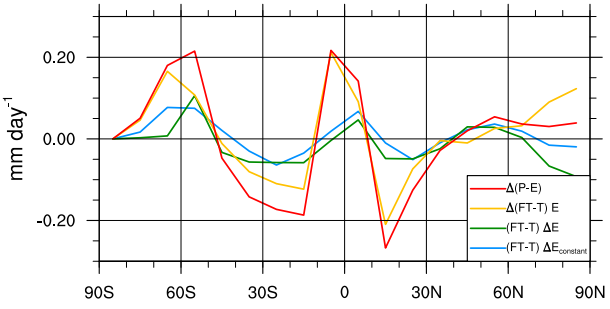

FIG. 3. Zonal mean change in the precipitation minus evaporation, $\Delta(\mathbf{P}-\mathbf{E})$, the portion of this change due to (local and remote) changes in evaporation, $(\mathbf{FT}-\mathbf{T})\Delta\mathbf{E}$, the portion of this change due to a spatially constant evaporation change, $(\mathbf{FT}-\mathbf{T})\Delta\mathbf{E}_{\text{constant}}$, and the portion of this change due to changes in moisture transport, $\Delta(\mathbf{FT}-\mathbf{T})\mathbf{E}$. All quantities are annual means and are shown in units of mm day^{-1}.

$$\Delta\mathbf{P} \approx (\Delta\mathbf{M})\mathbf{E} + \mathbf{M}(\Delta\mathbf{E}), \tag{5}$$

where $(\Delta\mathbf{M})\mathbf{E}$ is the change in precipitation due to changes in transport, given that evaporation remains constant (Figs. 1d–f); and $\mathbf{M}(\Delta\mathbf{E})$ is the change in precipitation due to changes in evaporation (both local and remote) given that transport remains constant (Figs. 1g–i). Zonal means of annually averaged quantities over the ocean domain only are given in Fig. 2.

The key features of this decomposition can be summarized as follows:

- The change in precipitation due to changes in evaporation is always positive, and is relatively spatially homogeneous in the annual mean. This can only be true if the change in evaporation is (mostly) positive, which it is (see section 5).
- The change in precipitation due to changes in the transport (both changes in the convergence of remotely evaporated moisture and the divergence of locally evaporated moisture) is spatially inhomogeneous compared to the change due to increasing evaporation. Broadly, this term is positive over the equatorial Pacific, negative over the subtropics and portions of the midlatitudes, and moderately positive over the high latitudes.
- Over the tropics and subtropics, the change in the precipitation due to the transport term is greater than that due to the evaporation term.
- In the annual mean, increased precipitation in the middle and high latitudes is due to increases in both the transport and evaporation terms. Intensified precipitation in the winter hemisphere, however, is dominated by the evaporation term, which is more seasonally variable in the middle and high latitudes.

We continue considering why moisture transport changes with CO_2 doubling in section 5. First, however, we will show how the change in the difference between precipitation and evaporation, $\Delta(\mathbf{P}-\mathbf{E})$, is partitioned into changes in transport and changes in evaporation.

b. *Decomposing the change in $P-E$*

In this work, our focus is on $\Delta\mathbf{P}$, which we analyze using a Lagrangian linear matrix operator framework where evaporated moisture is rearranged by transport to produce a given spatial pattern of precipitation. For the sake of completeness, however, we consider the relationship of our work to that of Held and Soden (2006), who considered the change in precipitation minus evaporation, $P-E$. In the matrix operator framework, the change in $\Delta(\mathbf{P}-\mathbf{E})$ can be decomposed as

$$\Delta(\mathbf{P}-\mathbf{E}) = (\mathbf{FT}-\mathbf{T})\Delta\mathbf{E} + \Delta(\mathbf{FT}-\mathbf{T})\mathbf{E}, \tag{6}$$

where the first term on the right-hand side, $(\mathbf{FT}-\mathbf{T})\Delta\mathbf{E}$, is the part due to changes in evaporation and the second, $\Delta(\mathbf{FT}-\mathbf{T})\mathbf{E}$, is the part due to changes in transport.

This decomposition (shown in Fig. 3) reveals that both components of $\Delta(\mathbf{P}-\mathbf{E})$ display the canonical spatial pattern corresponding to "the wet get wetter, the dry get drier," where the subtropics dry while the tropics and midlatitudes moisten. The amplitude of the change in $\mathbf{P}-\mathbf{E}$ due to $\Delta\mathbf{E}$ is smaller than that due to $\Delta(\mathbf{FT}-\mathbf{T})$ globally, but for the NH midlatitudes. Also shown is $(\mathbf{FT}-\mathbf{T})\Delta\mathbf{E}_{\text{constant}}$, where $\Delta\mathbf{E}_{\text{constant}}$ is prescribed to be globally spatially invariant (increased by 2.5% K^{-1} above the preindustrial mean state). When the change in evaporation is prescribed to be constant, the change in $\mathbf{P}-\mathbf{E}$ for a given region simply depends on the difference $\mathbf{FT}-\mathbf{T}$ in the mean state: whether a given region tends to attract remote moisture more than it tends to export local moisture, or vice versa. When $\sum_j f_{ij}e_j > e_i$, the transport in

the preindustrial control imports more moisture into the region from remote sources than it exports away from local sources, and the region gets wetter; on the other hand, when $\sum_j f_{ij} e_j < e_i$, the transport in the preindustrial control exports away more moisture from local sources than it imports from remote sources, and the region dries. While this argument gives the correct spatial structure of $\Delta(\mathbf{P} - \mathbf{E})$, much of the magnitude of the change is contained within the $\Delta(\mathbf{FT} - \mathbf{T})\mathbf{E}$ term.

It is important to note that the perturbation matrix operator framework presented here is Lagrangian, and is not equivalent to the traditional Eulerian framework where the moisture convergence term $\nabla \cdot Q$ is partitioned into changes due to $\delta\mathbf{v}$ (dynamics) and δq (thermodynamics) (see, e.g., Seager et al. 2010). Changes in the transport operator, $\Delta(\mathbf{FT} - \mathbf{T})$, should not be construed to be equivalent to "dynamic" changes with warming, and changes in evaporation, $\Delta\mathbf{E}$, should not be considered to be equivalent to "thermodynamic" changes. While q increases at the C-C scaling rate with warming, E increases at a rate well below this due to energetic limitations at the surface (Boer 1993). Increasing E requires local changes in the relative humidity, surface winds, and temperature gradients (Richter and Xie 2008; Lorenz et al. 2010). Thus, $\Delta\mathbf{E}$ includes both thermodynamic and dynamic changes. Similarly, changes in the transport operators that we have introduced here are due to changes in moisture transport tied to a variety of factors, which we consider in detail in our ensuing analysis. Nonetheless, we emphasize that the Lagrangian framework presented here is consistent with Held and Soden (2006), but that the fixed transport assumption explains only a small fraction of the changes in $\mathbf{P} - \mathbf{E}$ and an even smaller fraction of the changes in $\mathbf{P}$. In the remainder of this work, we will refer to changes in $\mathbf{P}$ that result from changes in our matrix operators, $\Delta\mathbf{F}$ and $\Delta\mathbf{T}$, as those due to changes in moisture transport, and will refer to those due to $\Delta\mathbf{E}$ as changes due to evaporation.

5. Changes in locally sourced precipitation versus changes in remotely converged precipitation

To better understand how the precipitation change is partitioned, we subdivide it into changes in local evaporation, local moisture divergence, and remote moisture convergence. We substitute the definition of the operator $\mathbf{M}$ given by Eq. (4) into $\mathbf{P} = \mathbf{ME}$ and compute its perturbation as

$$\Delta\mathbf{P} = \Delta\mathbf{E} - \Delta(\mathbf{TE}) + \Delta(\mathbf{FTE}), \tag{7}$$

where the total change in the precipitation $\Delta\mathbf{P}$ is subdivided as follows: the part due to the change in local evaporation, $\Delta\mathbf{E}$ (Figs. 4d–f); the part due to the change in the divergence of locally evaporated moisture, $-\Delta(\mathbf{TE})$ (Figs. 4g–i); and the part due to the change in the convergence of remotely evaporated moisture, $\Delta(\mathbf{FTE})$ (Figs. 4j–l). Alternately, $\Delta(\mathbf{P} - \mathbf{E})$, the change in the net moisture convergence $\Delta(\nabla \cdot Q)$ in the fundamental equation of hydrology (see Peixoto and Oort 1992), can be written as the sum of the latter terms, the local moisture divergence $-\Delta(\mathbf{TE})$ and the remote moisture convergence $\Delta(\mathbf{FTE})$. Annually averaged zonal means of these quantities over the ocean domain only are shown in Fig. 5.

The change in evaporation is positive nearly everywhere (Figs. 4d–f), while the change in the local divergence $-\Delta(\mathbf{TE})$ is negative nearly everywhere (Figs. 4g–i). Both are fairly spatially homogeneous in the annual average. Over much of the globe, the increase in the divergence of locally evaporated moisture is equal and opposite to the local increase in evaporation (cf. Figs. 4d–f and 4g–i; see also Fig. 5). We return to the sum of these terms, the change in the local contribution to the precipitation, in section 5a.

While $\Delta\mathbf{E}$ and $-\Delta(\mathbf{TE})$ are relatively homogenous and do not have the distinct spatial structure of $\Delta\mathbf{P}$, the change in the convergence of remotely evaporated moisture, $\Delta(\mathbf{FTE})$ is very similar spatially to $\Delta\mathbf{P}$ (cf. Figs. 4a–c and 4j–l; see also Fig. 5). The largest differences between these terms are over the deep tropics and subtropics, where changes in precipitation due to changes in the export of locally evaporated moisture, $-\Delta(\mathbf{TE})$, are also important. In general, the deep tropics tend to receive more precipitation because both the local $[\Delta(\mathbf{E} - \mathbf{TE})]$ and remote contributions to the total precipitation increase. On the other hand, the subtropics tend to receive less precipitation because the local contribution declines; in some areas, the remote contribution declines and augments this tendency, whereas in others the remote contribution increases modestly. Nevertheless, in most of the subtropics, the remote contribution does not increase sufficiently to compensate for the increased export of locally sourced evaporation.

Over the middle and high latitudes, the remote contribution increases both annually and seasonally, and increases slightly in the respective winter hemisphere, compared to the annual mean. This increased convergence of remotely evaporated moisture into the middle and high latitudes is consistent with increased poleward transport of latent heat in a warmer climate (Held and Soden 2006; Hwang and Frierson 2010).

a. *The change in the local contribution to the precipitation*

The change in the local contribution to the precipitation, equal to the sum of the first two terms on the

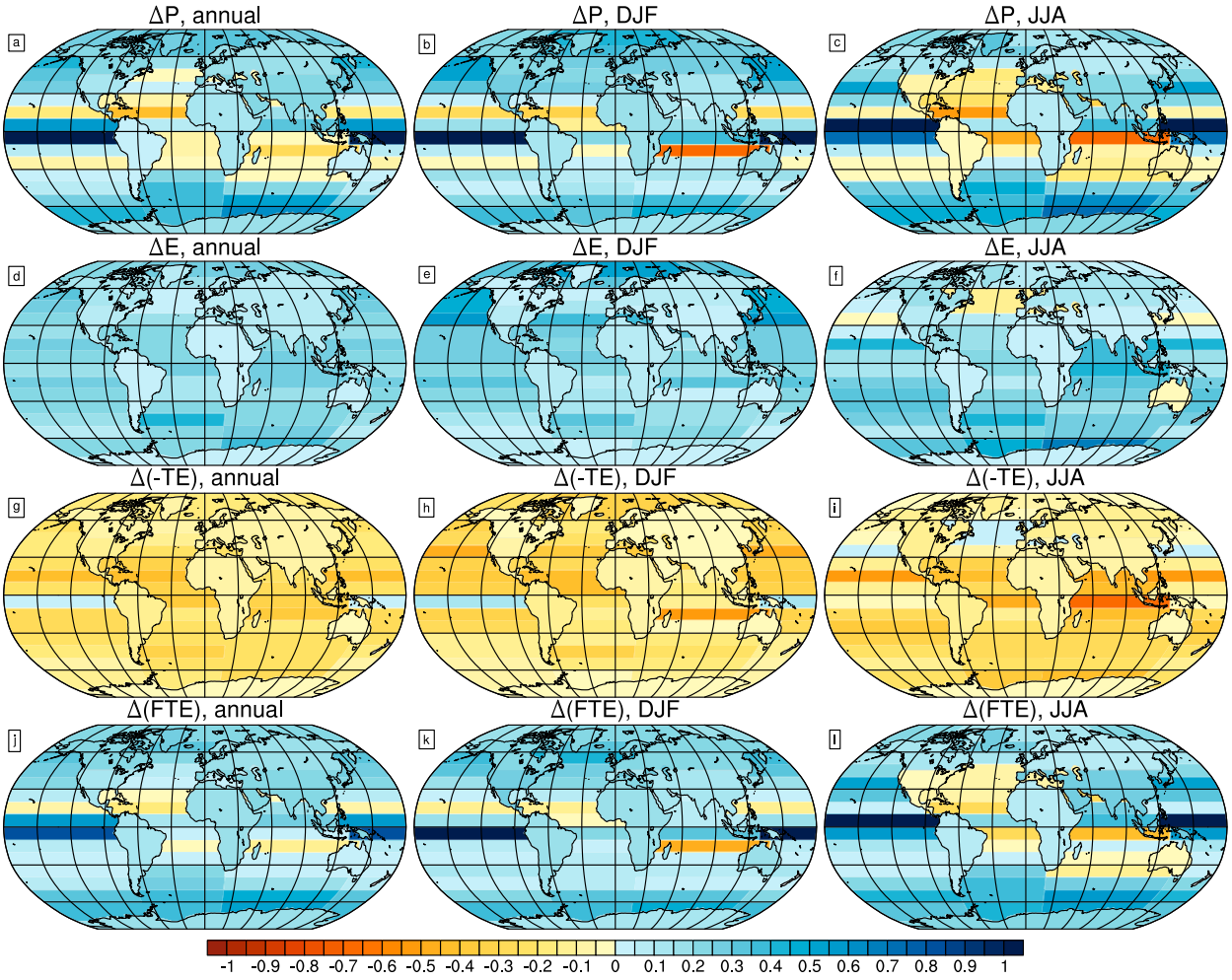

FIG. 4. Perturbation analysis of changes in the aerial hydrological cycle with CO_2 doubling, with the total change in precipitation decomposed as in Eq. (7). Shown are (a)–(c) the total change in precipitation (for comparison purposes), together with (d)–(f) the (local) change in evaporation, (g)–(i) the change in the divergence of locally evaporated moisture, and (j)–(l) the change in the convergence of remotely evaporated moisture. All quantities are shown (left) in the annual average and averaged over (middle) DJF and (right) JJA; all are in units of mm day^{-1}.

RHS of Eq. (7), is substantially smaller in magnitude than the change in the remote contribution (see Fig. 6; also cf. Figs. 7a–c and 4j–l). On average, the change in the local contribution makes up less than 20% of the total precipitation change in each tagged region.

Generally, the local contribution decreases in the tropics and subtropics over both land and ocean, and increases in the middle and high latitudes (Figs. 7a–c). There are, however, many exceptions. Over the oceans, the local contribution decreases over the Atlantic from 60°N to 40°S in the annual mean; on the other hand, the local contribution increases over the equatorial Pacific (0°–10°S) and Indian (0°–10°N) basins. For land regions, the local contribution decreases over South America, Africa, southern Eurasia, and southern North America, while it increases over the remaining land areas.

To understand why the change in the local contribution is so small, we subdivide it into one part due to changes in evaporation, and another due to changes in the moisture export fraction:

$$\Delta(\mathbf{E}-\mathbf{TE}) = (\mathbf{I}-\mathbf{T})\Delta\mathbf{E} + \Delta(\mathbf{I}-\mathbf{T})\mathbf{E}. \qquad (8)$$

The change in the local contribution due to changes in evaporation (Figs. 7d–f and 8) is positive almost everywhere and nearly spatially homogeneous in the annual mean; it is magnified in the middle and high latitudes in the winter hemisphere, particularly over the Arctic Ocean and North Pacific. On the other hand, the change in the local contribution due to changes in the export fraction (Figs. 7g–I and 8) is negative almost everywhere, is most prominent over the tropical oceans, and is

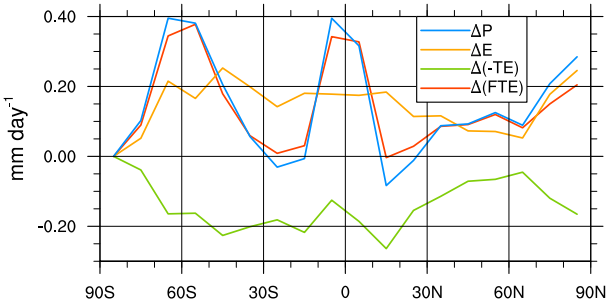

FIG. 5. Zonal mean over ocean regions of the annually averaged change in precipitation with CO_2 doubling and its perturbation decomposition as in Fig. 4.

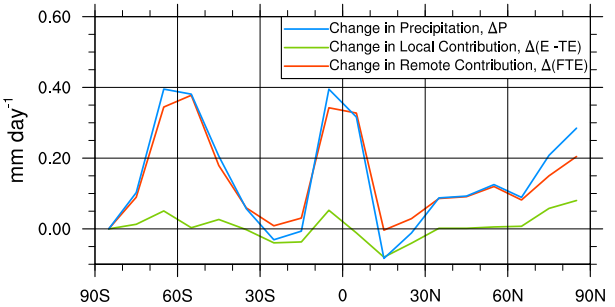

FIG. 6. The change in precipitation due to the change in the local contribution to the precipitation [$\Delta(\mathbf{E} - \mathbf{TE})$] and the change in the remote contributions to the precipitation [$\Delta(\mathbf{FTE})$]. All quantities are annually averaged zonal means (averaged over the ocean domain only), and shown in units of mm day^{-1}.

largest in JJA. The change in the local contribution to the precipitation is the residual sum of these two larger, opposing terms: evaporation increases nearly everywhere, which tends to increase precipitation from local moisture sources; on the other hand, the export fraction also increases nearly everywhere, which tends to decrease locally sourced precipitation. In the tropics and subtropics, the increased export wins out, and the local contribution to the precipitation decreases modestly in Eqm2×CO_2. In the middle and high latitudes, on the other hand, the local evaporation increase dominates over the effect of increased local moisture export, and the local contribution increases modestly.

The change in the export fraction, Δe_i, is shown in Fig. 9. Most striking is the homogeneity of the export fraction change, which is positive nearly everywhere. This increase in the export fraction acts to decrease locally sourced precipitation, but also acts to increase remotely sourced precipitation by enhancing remote moisture convergence into other regions. We assess the latter in the following section.

b. *The change in the remote contribution to the precipitation*

In Fig. 10, we show the relative change in the local contribution to total precipitation, $\Delta[(\mathbf{E} - \mathbf{TE})/\mathbf{P}]$, and the remote contribution to total precipitation, $\Delta(\mathbf{FTE}/\mathbf{P})$. With the exception of the high latitudes [where the fraction of the precipitation due to locally sourced moisture increases sharply due to more liquid water moisture sources; see Bintanja and Selten (2014) and Wegmann et al. (2015) for evidence of this in the Arctic], the fraction of the total precipitation due to remotely evaporated moisture increases globally in Eqm2×CO_2 while the fraction due to locally evaporated moisture decreases. Thus, remotely sourced moisture plays a larger role in precipitation in Eqm2×CO_2, a finding consistent with those of Gimeno et al. (2013).

We consider the change in remotely sourced precipitation by decomposing the change in the remote moisture convergence $\mathbf{FTE}$ as

$$\Delta(\mathbf{FTE}) = \mathbf{FT}(\Delta\mathbf{E}) + \mathbf{F}(\Delta\mathbf{T})\mathbf{E} + (\Delta\mathbf{F})\mathbf{TE}, \qquad (9)$$

so that the remote moisture convergence perturbation is subdivided into components due to changes in evaporation, changes in the export fraction, and changes in moisture convergence partitioning to other regions, respectively. As expected, changes in the evaporation tend to increase remote moisture convergence everywhere (Figs. 11d–f and 12), since more evaporation provides more moisture for converging elsewhere. Changes in the moisture export fraction also tend to increase remote moisture convergence (Figs. 11g–i and 12), although this increase is slightly less than that due to enhanced evaporation. Since the export fraction increases nearly everywhere (recall Fig. 9), less moisture precipitates locally and more moisture is available for converging remotely.

Changes in the remote moisture convergence due to changes in the partitioning of moisture between remote regions, $\Delta\mathbf{F}$ (Figs. 11j–l and 12), are much more spatially heterogeneous and somewhat larger in magnitude than the changes due to $\Delta\mathbf{E}$ and $\Delta\mathbf{T}$. In the high latitudes and much of the midlatitudes, this term tends to increase remote moisture convergence whereas in the subtropics and tropics this term tends to decrease it. This spatial pattern is consistent with enhanced poleward moisture transport with CO_2-induced warming (Hwang and Frierson 2010). The major exceptions are over the equatorial Pacific and Indian basins, with the increase in precipitation in the Pacific greatly exceeding that in the Indian, and over Africa and southern Eurasia. Moreover, this term tends to decrease precipitation preferentially over much of the Atlantic basin, compared to the Pacific and Indian basins.

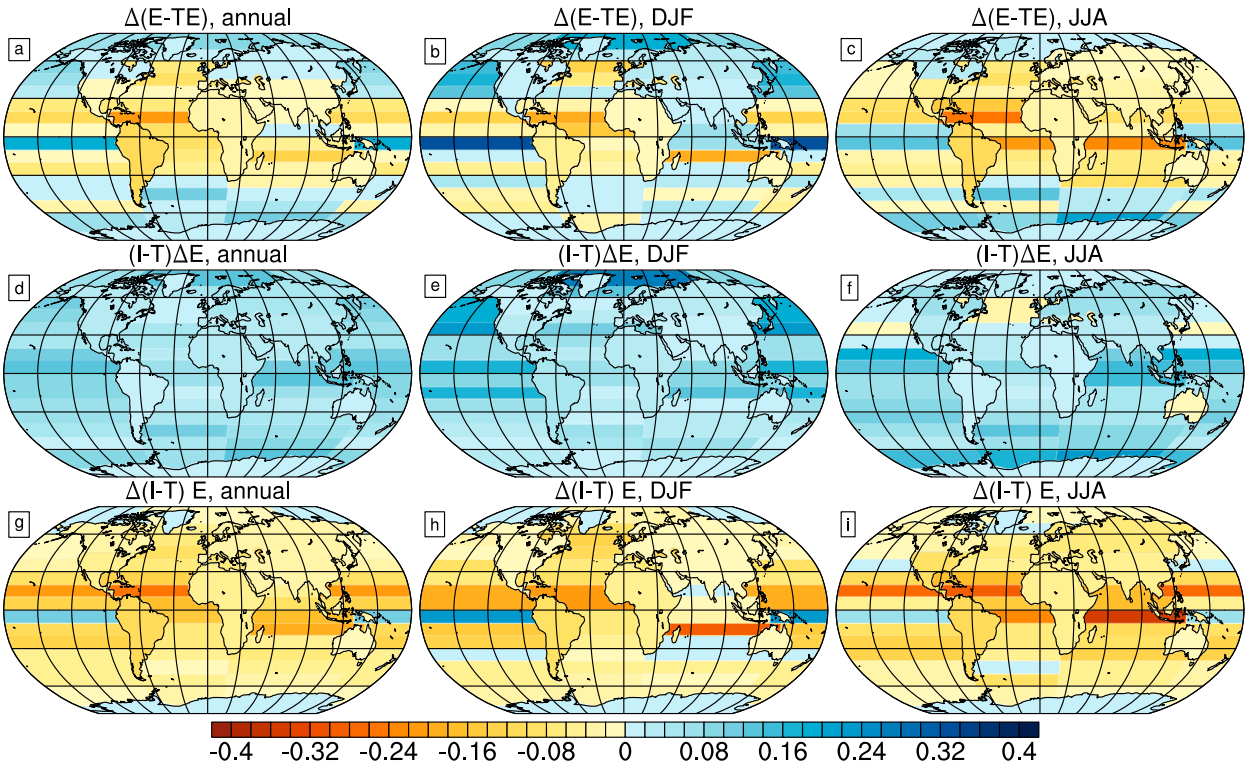

FIG. 7. (a)–(c) The change in the local precipitation contribution $\Delta(\mathbf{E}-\mathbf{TE})$, decomposed into (d)–(f) the part of the local precipitation change due to the change in the evaporation $(\mathbf{I}-\mathbf{T})\Delta\mathbf{E}$ and (g)–(i) the part due to changes in moisture export fraction $\Delta(\mathbf{I}-\mathbf{T})\mathbf{E}$. Quantities are shown for (left) the annual mean and for (middle) DJF and (right) JJA, and are in units of mm day^{-1}.

To gain further insight into how changes in the convergence of remotely evaporated moisture contribute to precipitation changes, we may partition $\Delta(\mathbf{FTE})$ using a physically motivated decomposition of matrix $\mathbf{F}$. In general, $\mathbf{F}$ is subdivided into n contributions such that $\Delta(\mathbf{FTE})$ is separated into n terms, each of which is due to some component $\mathbf{F}_n$:

$$\Delta(\mathbf{FTE}) = \Delta\left(\sum_n \mathbf{F}_n\mathbf{TE}\right) = \sum_n \Delta(\mathbf{F}_n\mathbf{TE}). \qquad (10)$$

To separate the remote moisture convergence into ocean and land sources and sinks, we decompose $\mathbf{F}$ as

$$\Delta(\mathbf{FTE}) = \Delta(\mathbf{F}_{\text{O-O}}\mathbf{TE}) + \Delta(\mathbf{F}_{\text{O-L}}\mathbf{TE}) + \Delta(\mathbf{F}_{\text{L-O}}\mathbf{TE}) + \Delta(\mathbf{F}_{\text{L-L}}\mathbf{TE}), \qquad (11)$$

where the terms on the right-hand side are due to 1) moisture sourced from the ocean that also converges over the ocean, 2) moisture sourced from the ocean that converges over land, 3) moisture sourced from land that converges over the ocean, and 4) moisture sourced from land that also converges over land.

To understand changes in the remote moisture convergence over ocean, term (1) in Eq. (11) above, we decompose $\Delta(\mathbf{F}_{\text{O-O}}\mathbf{TE})$ into an intrabasin term, where moisture precipitates in the same basin in which it evaporates, and an interbasin term, where moisture precipitates in a different basin than the basin where it evaporates:

$$\Delta(\mathbf{F}_{\text{O-O}}\mathbf{TE}) = \Delta(\mathbf{F}_{\text{intrabasin}}\mathbf{TE}) + \Delta(\mathbf{F}_{\text{interbasin}}\mathbf{TE}). \qquad (12)$$

Shown in Figs. 13a, 13b, and 14, the changes in the interbasin and intrabasin moisture convergence are of roughly similar magnitude, although the latter greatly

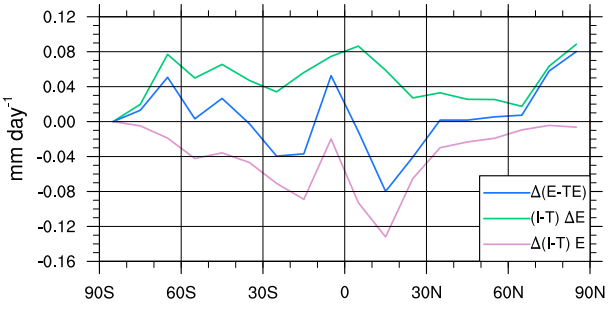

FIG. 8. Zonal mean over ocean regions of the annually averaged change in the local contribution to the precipitation and its perturbation decomposition as in Fig. 7.

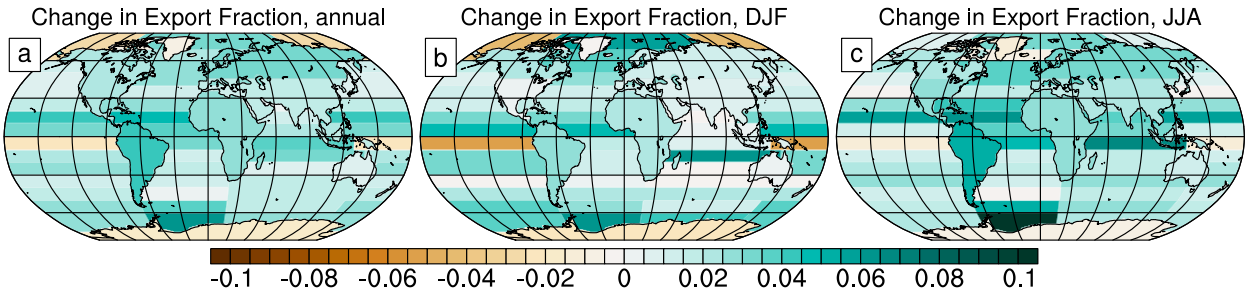

FIG. 9. The change in the export fraction e_i for (a) the annual mean, (b) DJF, and (c) JJA.

dominates the mean state (as shown in Part I). Furthermore, the interbasin moisture convergence increases globally, with the largest increases over the Southern Ocean and equatorial Pacific, and smaller increases over the Pacific and the northern Indian basins. In contrast, the intrabasin moisture convergence term is more spatially heterogeneous, with decreased convergence over the subtropics over all three basins and increased convergence over the middle and high latitudes. Intrabasin-sourced equatorial precipitation increases most strongly over the Pacific, modestly over the Indian, and not at all over the Atlantic. As noted earlier, the change in the remote moisture convergence is consistent with a pattern of increased convergence over the equatorial regions, midlatitudes, and polar regions, and decreased convergence over the subtropics. Indeed, the major difference between the intrabasin and interbasin components of the remote moisture convergence change is the change in the subtropics, which is weakly positive in the interbasin component, but mostly negative in the intrabasin component. Thus, precipitation decreases in the subtropics are due to increased export of locally evaporated moisture and decreasing intrabasin moisture convergence, both of which are incompletely compensated for by increased local evaporation and increased interbasin moisture convergence.

We further extend the decomposition from Eq. (12) by subdividing the intrabasin component into "near" and "far" components (moisture originates in a latitude band adjacent to where it precipitates, and not adjacent to where it precipitates, respectively):

$$\Delta(\mathbf{F}_{\text{O-O}}\mathbf{TE}) = \Delta(\mathbf{F}_{\text{inter}}\mathbf{TE}) + \Delta(\mathbf{F}_{\text{intra,near}}\mathbf{TE}) + \Delta(\mathbf{F}_{\text{intra,far}}\mathbf{TE}). \quad (13)$$

Shown in Figs. 13d, 13e, and 14, this decomposition successfully separates the intrabasin moisture convergence into a part that decreases over much of the

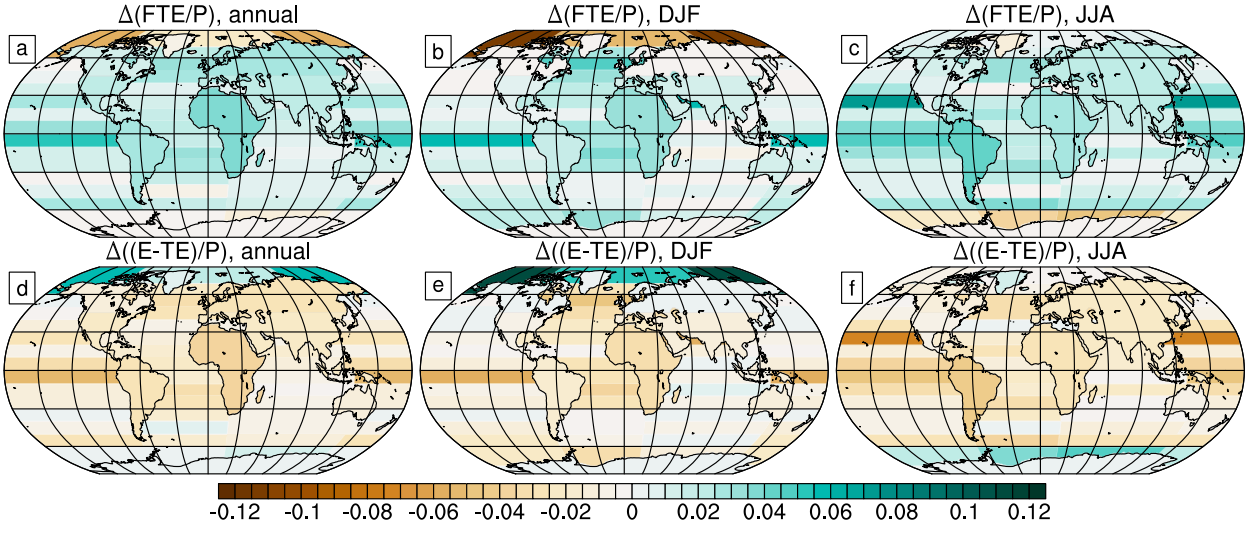

FIG. 10. (a)–(c) The change in the fraction of the total precipitation originating remotely [$\Delta(\mathbf{FTE}/\mathbf{P})$] and (d)–(f) the change in the fraction of the total precipitation originating locally $\Delta[(\mathbf{E} - \mathbf{TE})/\mathbf{P}]$), shown for (left) the annual mean and for (middle) DJF and (right) JJA.

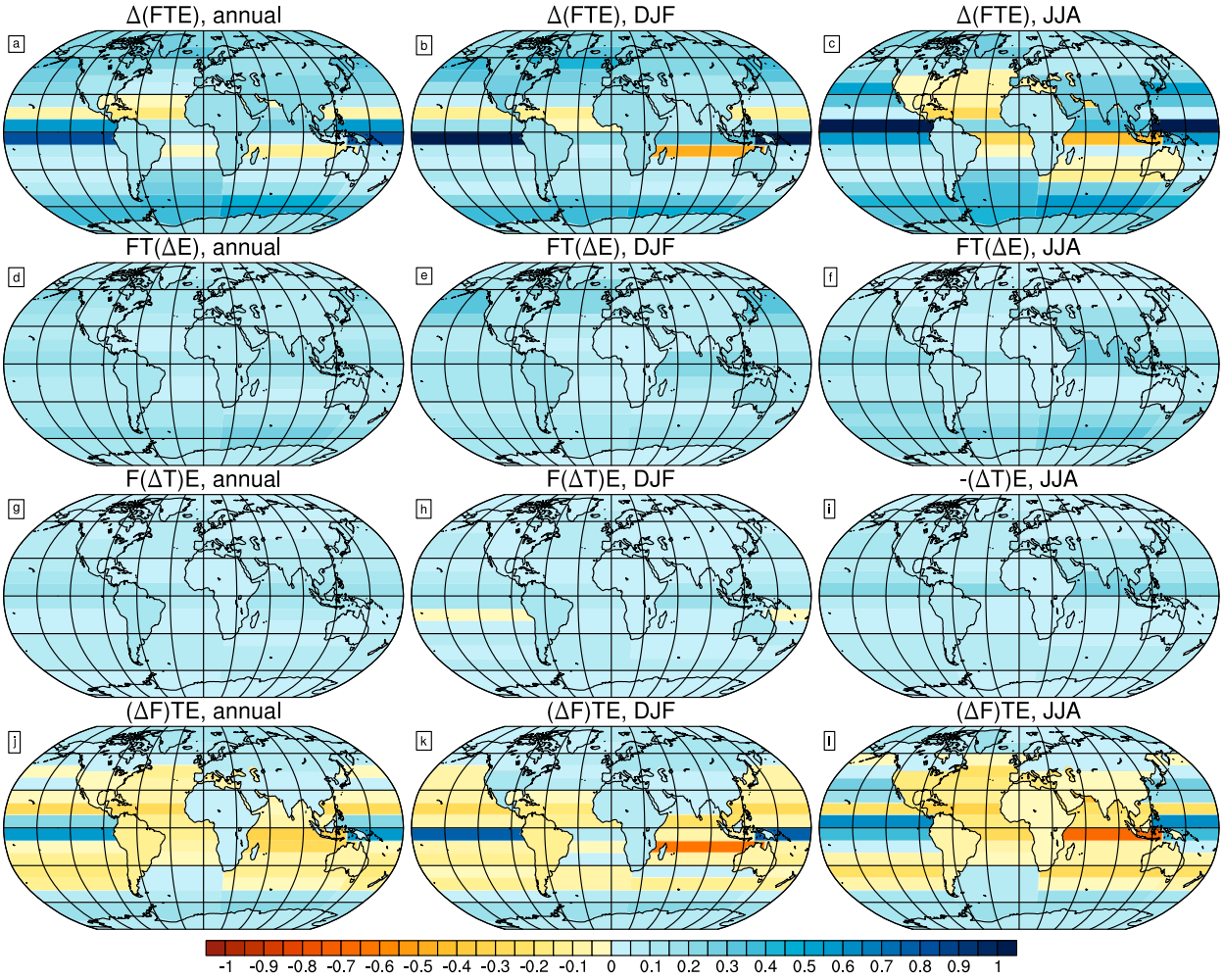

FIG. 11. Decomposition of the remote moisture convergence term, Δ(**FTE**), as given in Eq. (9): (a)–(c) the entire term, (d)–(f) that due to changes in evaporation **FT**(Δ**E**), (g)–(i) that due to changes in moisture export **F**(Δ**T**)**E**, and (j)–(l) that due to changes in the partitioning of remotely evaporated moisture between sink regions (Δ**F**)**TE**. Each term is shown for (left) the annual mean and for (middle) DJF and (right) JJA. All quantities are in units of mm day^{-1}.

globe (the near component) and another that increases over much of the globe (the far component). Indeed, the former decreases everywhere except over the north and equatorial Pacific, the Atlantic sector of the Southern Ocean, and a small swath of the equatorial Indian; the latter increases everywhere, except for a small region over the subtropical Atlantic and equatorial Indian basins. This suggests a systematic decrease in moisture convergence from adjacent regions, and a corresponding increase in moisture convergence from more remote regions. Combined with the greater export fraction, the greater fraction of precipitation due to remotely sourced moisture, and a greater interbasin moisture convergence, this indicates that moisture is transported farther in the Eqm2×CO_2 experiment relative to piC.

6. Understanding moisture transport changes in Eqm2×CO_2 using heuristic models

Several lines of evidence point to an increased distance between moisture source and sink regions in Eqm2×CO_2 relative to piC. First, the fraction of locally evaporated moisture that is exported increases globally (Fig. 9), and the fraction of the precipitation due to remotely sourced moisture increases nearly globally (Fig. 10). Second, the convergence of remotely evaporated moisture shifts toward longer distances between source (evaporation) and sink (precipitation) regions: interbasin moisture convergence increases everywhere (Figs. 13b and 14) and the part of the intrabasin moisture convergence that originates as evaporation from an adjacent latitude band decreases almost everywhere

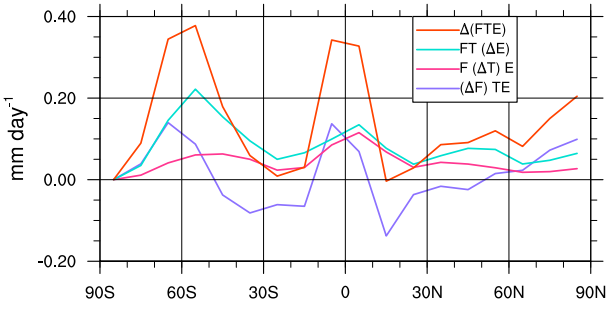

FIG. 12. Zonal mean over ocean regions of the annually averaged change in the remote moisture convergence and its perturbation decomposition as in Fig. 11.

(Figs. 13c and 14), while the part that originates as evaporation from more distant latitude bands increases (Figs. 13d and 14).

The global extent of these changes suggests that a simple, robust mechanism is responsible. In the ensuing analysis, we show that this increase in the length scale of moisture transport corresponds to an increase in the moisture residence time, which arises from a decline in the tendency of atmospheric moisture to precipitate.

a. Adjustment time scales in a one-box model

First, consider a self-contained (i.e., no moisture influx) domain with an evolving atmospheric moisture content $Q(t)$ and (constant) evaporation rate E_0. Following Trenberth (1998) and Bosilovich et al. (2005), the precipitation can be written as a depletion tendency γ multiplied by the total moisture. Thus, Q must satisfy the ordinary differential equation (ODE)

$$\frac{dQ}{dt} = E_0 - \gamma Q. \tag{14}$$

If $Q(t=0) = 0$, the solution is $Q(t) = (E_0/\gamma)(1 - e^{-\gamma t})$. The adjustment time scale for Q to approach the steady-state solution $Q = E_0/\gamma$ is $\tau = 1/\gamma$.

If Q increased at the C-C rate with a fixed moisture depletion tendency coefficient γ, then the precipitation, γQ, would also scale at the C-C rate. Therefore, the fact that precipitation increases at less than the C-C rate (as noted throughout the literature) implies that the moisture depletion tendency γ must decrease (see Trenberth 1998; Bosilovich et al. 2005; van der Ent and Savenije 2011). This, in turn, corresponds to a decrease in the rate of moisture cycling or, analogously, an increase in the atmospheric moisture residence time scale τ, as we have shown above. Intuition suggests that increasing the moisture residence time would also increase the atmospheric moisture transport length scale, the distance between moisture source and sink regions. We demonstrate this below.

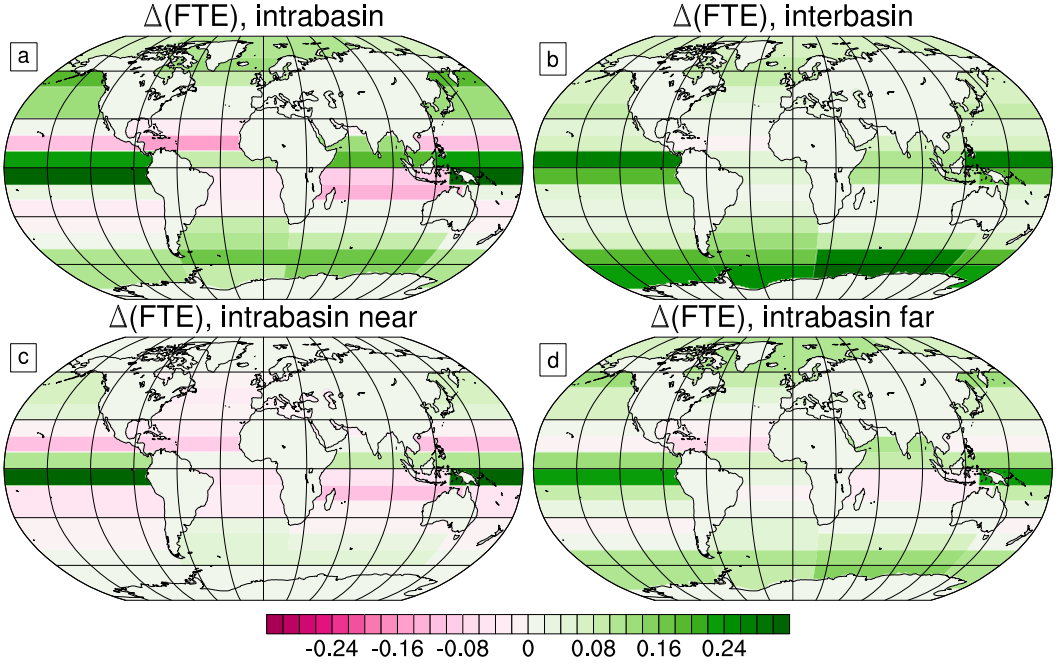

FIG. 13. Another decomposition of the $\Delta(\mathbf{F}_{O\text{-}O}\mathbf{TE})$ into (a) intrabasin (within basin) and (b) interbasin (between basin) components, with the intrabasin component further subdivided into (c) "near" and (d) "far" components as in Eq. (13). All quantities are in units of mm day^{-1}.

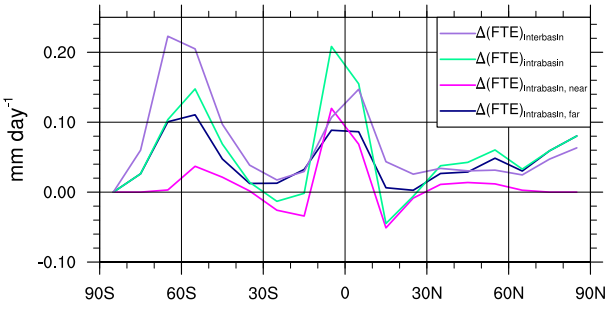

FIG. 14. Zonal mean over ocean regions of the annually averaged change in the ocean-to-ocean remote moisture convergence as in Fig. 13.

b. *The length scale in a spatially continuous model*

Consider a one-dimensional continuous spatial domain in which the vertically integrated atmospheric moisture is $Q(x)$. Here, the atmospheric moisture increases due to evaporation, $E(x)$, decreases due to depletion by precipitation, γQ, and is advected by atmospheric motions, $v(x)$:

$$\frac{\partial Q}{\partial t} = E(x) - \nabla \cdot (vQ) - \gamma Q. \tag{15}$$

If v and E are assumed to be constant over the spatial domain, Eq. (15) may be written as

$$\frac{\partial Q}{\partial t} = E - v\frac{\partial Q}{\partial x} - \gamma Q. \tag{16}$$

If $Q(x=0)=0$, we obtain the steady-state solution $Q(x) = E_0/\gamma(1 - e^{-\gamma x/v})$, where the advective length scale is $\lambda \equiv v/\gamma$. A decline in γ will cause the moisture transport length scale to increase, thereby shifting the aerial hydrological cycle toward greater distances between source (evaporation) and sink (precipitation) regions. In the appendix, we use an n-box model to show with greater rigor that a decline in the moisture depletion tendency γ will shift precipitation toward greater distances between moisture sources and sinks.

7. Discussion and conclusions

In this study, we have used a Lagrangian matrix operator framework to consider perturbations in the aerial hydrological cycle due to quasi-equilibrium CO_2 doubling. This work presents a different perspective, complementary to Eulerian frameworks, for evaluating hydrological cycle changes by utilizing the information made available by numerical WTs implemented in a GCM. Our analysis synthesizes the two governing principles of CO_2-induced hydrological cycle change: that atmospheric moisture increases at the C-C rate with temperature (approximately 7% °C^{-1}), and that energetic constraints on E and P cap their increase well below the C-C rate. Both of these principles are linked by the moisture depletion tendency γ (Trenberth 1998; Bosilovich et al. 2005), which must decline if both are to be satisfied simultaneously. A decline in the moisture depletion tendency γ corresponds to an increase in moisture residence time and, as we have shown, an increase in the length scale of moisture transport.

If E, P, and specific humidity q all increased at the same rate with increasing temperature, and the circulation remained relatively fixed, γ would remain constant and much of the change in precipitation would arise from the evaporation change itself, that is, $\Delta\mathbf{P} \approx \mathbf{M}(\Delta\mathbf{E})$. In other words, the total precipitation change would only depend on changes in the spatial pattern of evaporation, which depend on changes in the surface energy budget. In reality, both precipitation and evaporation increase with temperature at a slower rate than the specific humidity; as a result of this incongruity, the rate at which moisture is removed from the atmosphere must slow or, equivalently, γ must decrease. The decrease in the moisture depletion tendency, then, increases the export fraction, and shifts the precipitation contribution due to remotely evaporated moisture toward longer distances between source and sink regions. This manifests itself in the $(\Delta\mathbf{M})\mathbf{E}$ term, which is as important to the total precipitation change as the $\mathbf{M}(\Delta\mathbf{E})$ term.

A corollary of this finding is that dynamic shifts in general circulation features, particularly the expansion of the subsiding regions of the Hadley circulation and the poleward shift in the storm track that accompanies it, are expected with this increase in the advective length scale of moisture transport. Widening of the subtropics corresponds to a larger source region from which water can evaporate along the way to the deep tropics, which is consistent with an increased transport length scale. Additionally, increasing the transport length scale will also push the midlatitude precipitation maximum poleward, since water from subtropical source regions will travel further. In other words, increasing the advective length scale of moisture transport produces hydrological cycle perturbations with CO_2-induced warming that are consistent with the dynamical perturbations observed in a wide range of GCMs.

As our results show, increasing evaporation without changing moisture transport results in a nearly uniform pattern of increased precipitation, with a notable maximum in the middle and high latitudes in winter. In fact, much of the increased precipitation in the extratropics in Eqm2×CO_2 is due to increased evaporation in the

subtropics and midlatitudes that is transported poleward in a manner similar to that in the mean state. In the tropics, however, changes in evaporation cannot explain the pattern of strengthening equatorial precipitation and decreasing subtropical precipitation. In this regard, changes in moisture transport are essential for creating the distinct spatial pattern of precipitation change associated with CO_2-induced warming.

Given that the advective length scale of moisture transport is $\lambda = \upsilon/\gamma$, increased moisture transport distances would also result if the circulation were to intensify. However, studies of general circulation perturbations with CO_2-induced warming suggest that its tendency in the tropics and subtropics is to slow down, not speed up (see, e.g., Vecchi and Soden 2007). Thus, perturbations in the general circulation tend to decrease the advective length scale of moisture transport, at least at lower latitudes, and counteract the effect of the decreasing moisture depletion tendency γ. Our results suggest, however, that weakening of the general circulation does not negate the effect of decreased γ, and the advective length scale of moisture increases nearly everywhere. In Singh et al. (2016b) we show that CMIP5 perturbation experiments suggest a robust increase in the advective moisture length scale in all state-of-the-art GCMs, as evidenced by near-universal intermodel agreement that the Atlantic–Pacific salinity contrast will increase as the planet warms.

The change in precipitation due to $\Delta\mathbf{E}$ is not equivalent to the so-called thermodynamic effect of increased atmospheric moisture. As others have already shown, increased atmospheric moisture cannot account for how E and P change independently (Allen and Ingram 2002; Held and Soden 2006). Likewise, the change in precipitation due to changes in the matrix operator $\mathbf{M}$ and its constituents are not due to changes in dynamics (i.e., changes in $\delta\mathbf{v}$), per se, but changes in moisture transport. Here, we have argued that changes in moisture transport are linked to an increase in the moisture transport length scale, which arises naturally from the decrease in the atmospheric moisture depletion tendency that characterizes CO_2-induced warming.

The local and remote contributions to the precipitation perturbation are each impacted differently by this advective length scale increase. Surprisingly, we find that the local contribution to the precipitation changes very little in the Eqm2×CO_2 experiment relative to piC, despite the fact that the export fraction increases almost everywhere. This can be explained, however, by a compensating increase in the local evaporation: even though more locally evaporated moisture is transported away from where it evaporates as the advective length scale of moisture transport increases, local evaporation increases sufficiently to counteract this. As a result, the change in the local contribution makes up less than 20% of the total precipitation perturbation. This leaves the change in the convergence of remotely evaporated moisture (the remote contribution) as the dominant component of the total precipitation perturbation.

These changes in the local and remote contributions to the precipitation are not uniform among the basins. Overall, the Atlantic basin dries the most ($\Delta E > \Delta P$) while the Pacific slightly moistens ($\Delta E < \Delta P$). Over the Atlantic, surprisingly, remote moisture convergence does not increase over the deep tropics. Thus, even though the Atlantic experiences subtropical drying similar to the other basins, there is no increasing equatorial precipitation to compensate for this drying. Over the Pacific, equatorial precipitation increases primarily because changes in moisture partitioning favor convergence over this area. In addition, the effect of increasing the advective length scale of moisture transport is least apparent over the subtropical and midlatitude Pacific, with intrabasin moisture convergence from adjacent tagged regions relatively unaffected. We speculate that the Pacific is relatively impervious, in part because of its substantial zonal extent: any moisture evaporated over the Pacific basin that is advected zonally likely remains over the Pacific basin when it precipitates, despite any modest transport length scale changes.

Over the continents, the relative contribution of the local and remote portions of the precipitation perturbation varies by region. Mostly, the local contribution to the precipitation declines, with the exception of the high latitudes, where the local contribution increases modestly. The remote contribution, on the other hand, increases over all land regions primarily because ocean-to-land moisture convergence increases. In general, the sum of these two competing tendencies determines whether precipitation increases or decreases over a given landmass. Over the polar regions, where both the local and remote contributions increase, precipitation always increases. Over most other landmasses, the increase in the remote contribution wins out over the declining local contribution, and precipitation increases year-round. Exceptions are over South America, and, seasonally, over southern North America and Australia, where the declining local contribution is not sufficiently compensated for by the increasing remote contribution, and precipitation declines.

Our findings have important implications for isotope studies. Our GCM WT experiments confirm that the advective length scale of moisture transport changes with temperature. In warmer temperatures, as in the Eqm2×CO_2 experiment, the advective length scale

increases relative to piC; similarly, in cooler temperatures, the advective length scale is expected to decrease. From the perspective of moisture from the subtropics that is transported poleward, both the temperature at which it evaporated and the time spent in the aerial hydrological cycle impact the isotopic signature; both of these components, however, depend on temperature in both a local and global sense. This suggests, then, that back-of-the-envelope calculations of state variables from isotope data are ill advised, as these secondary effects of temperature and its impact on transport may not be easily distilled into a simple model. Thus, we contend that isotope-enabled GCM studies are essential for interpreting isotope proxy records, particularly those in which global temperatures are very different from that in the present climate.

We conclude by pointing out the major caveat associated with this and any study using numerical WTs in GCMs, namely that the findings we present here are limited by the ability of our GCM to model the aerial hydrological cycle with fidelity. Thus, the conclusions presented here should be verified with additional GCM studies, including those that are isotope-enabled.

Acknowledgments. HKAS thanks colleagues Dennis Hartmann and Chris Bretherton for feedback; and acknowledges support from the U.S. DOE CSGF. CMB acknowledges support from the National Science Foundation (NSF) through Grant PLR-1342497. All authors acknowledge high-performance computing support from Yellowstone (ark:/85065/d72d3xhc) provided by NCAR's Computational and Information Systems Laboratory, sponsored by the NSF.

APPENDIX

Time Scales and Length Scales in an *n*-Box Model

We use an n-box model to demonstrate that a moisture residence time scale increase directly corresponds to a greater fraction of moisture originating further afield and a smaller fraction originating nearby. Consider a system of n atmospheric boxes of length L (Fig. A1), each with moisture content $Q_i(t)$ and evaporation rate E_i. As for the single box models (see section 6), the precipitation is proportional to the box's moisture content and is written as γQ_i. Additionally, moisture is advected between boxes by some advective velocity v. This yields a system of n coupled ODEs:

$$\begin{aligned}
\frac{dQ_1}{dt} &= E_1 - \gamma Q_1 - \frac{v}{L}Q_1 \\
\frac{dQ_2}{dt} &= E_2 - \gamma Q_2 - \frac{v}{L}Q_2 + \frac{v}{L}Q_1 \\
&\cdots \\
\frac{dQ_n}{dt} &= E_n - \gamma Q_n - \frac{v}{L}Q_n + \frac{v}{L}Q_{n-1},
\end{aligned} \tag{A1}$$

with an advective time scale of $\tau = 1/(\gamma + v/L)$. Once again, it is clear that decreasing the precipitation tendency would increase the residence time scale. Additionally, the moisture residence time may also be increased by decreasing the advection velocity v or increasing the box length L.

The steady-state solution ($dQ_i/dt = 0$) for the nth box may be written as the finite series

$$Q_n = \frac{1}{\beta}\sum_{j=1}^{n}\left(\frac{v}{L\beta}\right)^{n-j}E_i, \tag{A2}$$

where $\beta = \gamma + v/L$ is the moisture cycling rate and $1/\beta$ is the time scale τ.

To show that the fraction of moisture in the nth box coming from the pth (where p is sufficiently small) increases as γ decreases, we use Eq. (A2) to compute the fraction of moisture in the nth box that comes from the pth box:

$$F_{n,p} = \frac{\left(\frac{v}{L\beta}\right)^{n-p}E_p}{\sum_{i=1}^{n}\left(\frac{v}{L\beta}\right)^{n-i}E_i}. \tag{A3}$$

To simplify the mathematics, let all $E_i = E_0$ and define the nondimensional parameter $\xi \equiv [(v/L)/\gamma + (v/L)] = v/L\beta$, noting that $|\xi| < 1$ for all $\gamma > 0$. Then, $F_{n,p}$ can be written as

$$F_{n,p} = \frac{(\xi)^{n-p}}{\sum_{i=1}^{n}(\xi)^{n-i}}. \tag{A4}$$

Using the Taylor series expansion, valid for $|x| < 1$, $1/(1-x) = 1 + x + x^2 + x^3 + \ldots$, Eq. (A4) may be well approximated as $F_{n,p} \approx \xi^{n-p}(1-\xi)$. Taking the partial derivative of $F_{n,p}$ with respect to β yields

$$\frac{\partial F_{n,p}}{\partial \beta} = \frac{1}{\beta}\left[(n-p+1)\left(\frac{v}{L\beta}\right)^{n-p+1} - (n-p)\left(\frac{v}{L\beta}\right)^{n-p}\right], \tag{A5}$$

which is less than zero when p is less than some critical value p_c:

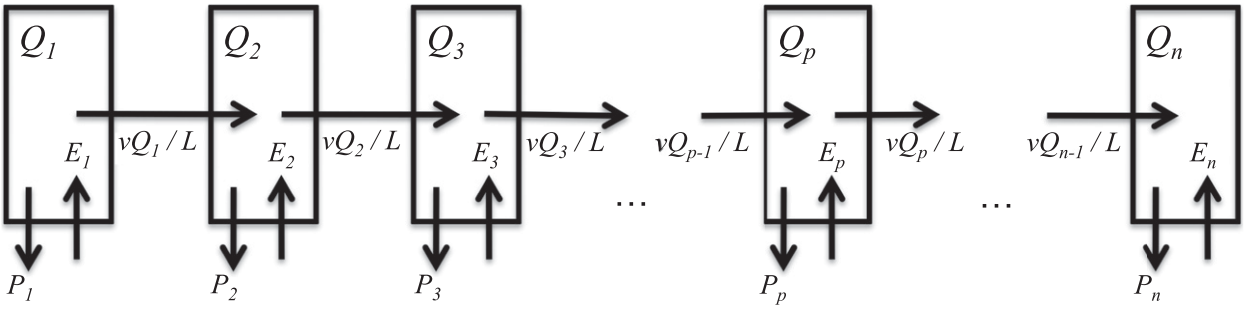

FIG. A1. Schematic of the n-box model used to study moisture transport length scales. The length of each box is L and the moisture content is Q_i. Moisture is replenished by evaporation E_i and is depleted by precipitation $P_i = \gamma Q_i$. Moisture flux between boxes is unidirectional at some uniform advective velocity v. A smaller three-box model, as described in the text, consists of only the first three boxes on the left-hand side.

$$p_c = n - \frac{v}{L\beta - v} = n - \frac{v}{L\gamma}. \tag{A6}$$

Therefore, for boxes that satisfy $1 \le p < p_c$, $F_{n,p}$ increases as γ decreases, indicating that decreasing the precipitation tendency, and thereby the moisture cycling rate, will increase the fraction of moisture in box n that comes from these distant boxes. Conversely, for boxes that satisfy $p_c < p \le n$, the same decrease of the precipitation tendency will decrease the fraction of

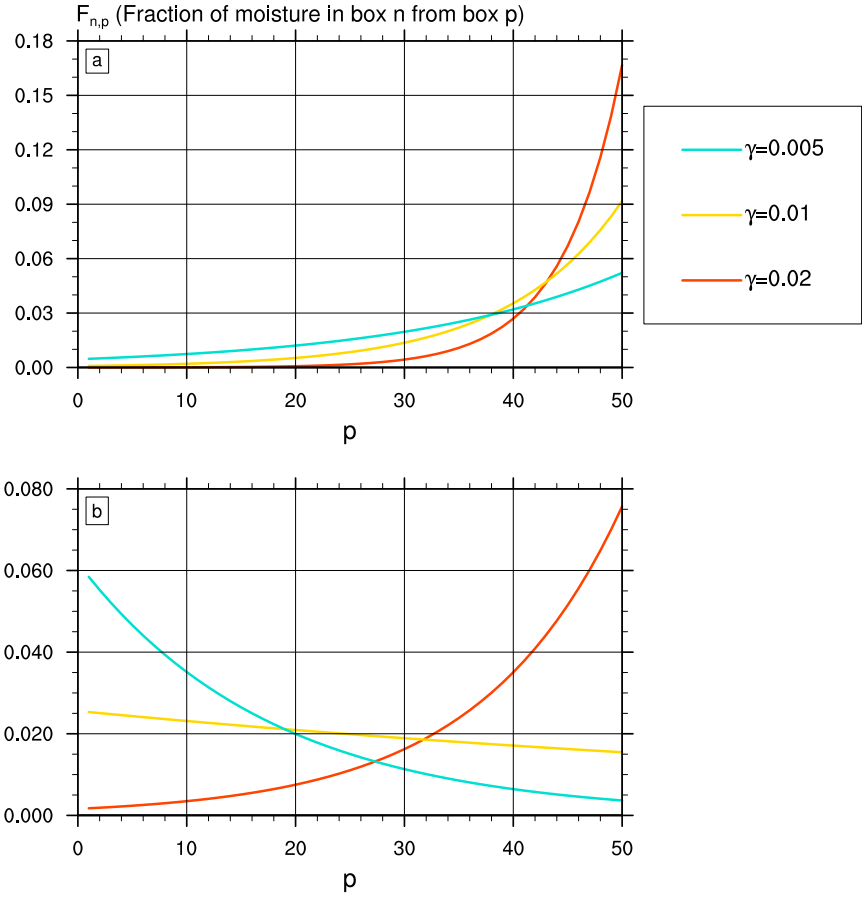

FIG. A2. The value of $F_{n,p}$, the fraction of moisture in box n originating from box p, for three different values of the precipitation tendency γ (given in s^{-1}): (a) with constant evaporation in each box (i.e., $E_p = E_0$) and (b) with evaporation decreasing geometrically with the box number, $E_p = (0.9)^{p-1}E_0$. Other constants are as follows: $v = 10\,m\,s^{-1}$, $L = 100\,m$, and $n = 50$.

moisture in box n that comes from these proximal boxes. Furthermore, decreasing γ will decrease this critical value p_c; in other words, decreasing the precipitation tendency will also tend to shift the range of boxes at which $\partial F_{n,p}/\partial\gamma < 0$ to boxes that are even more distant.

In Fig. A2, we present some distributions of $F_{n,p}$ as a function of box p, using several different values of the precipitation tendency γ; results are shown with $n = 50$ boxes, $L = 100\,\text{m}$, and $v = 10\,\text{m}\,\text{s}^{-1}$. When evaporation is constant across boxes (Fig. A2a), decreasing γ tends to flatten the distribution of $F_{n,p}$, decreasing the fraction of moisture in box n that originates in proximal boxes and increasing the fraction that originates in distant boxes. Furthermore, decreasing γ tends to decrease the value of p_c that separates regions where $F_{n,p}$ increases and where it decreases; in particular, the solutions for $\gamma = 0.01\,\text{s}^{-1}$ and $\gamma = 0.02\,\text{s}^{-1}$ intersect at larger p than the solutions for $\gamma = 0.005\,\text{s}^{-1}$ and $\gamma = 0.01\,\text{s}^{-1}$.

Suppose that the evaporation is allowed to vary between boxes such that $E_p = (0.9)^{p-1}E_0$, giving a geometric decrease in evaporation with box number. In this case, the moisture fraction from distant boxes increases and the moisture fraction from proximal boxes decreases as γ decreases (Fig. A2b). As γ decreases, p_c also decreases, indicating a shift toward more distant source regions. Compared to the constant evaporation case, however, both these effects are amplified (i.e., $\partial F_{n,p}/\partial\gamma$ is much larger). Thus, small changes in the precipitation tendency have a much larger effect on the moisture source region distribution for the nth box when the evaporation is allowed to decrease with box number, compared to the case when the evaporation is held constant.

REFERENCES

Allan, R., B. Soden, V. John, W. Ingram, and P. Good, 2010: Current changes in tropical precipitation. *Environ. Res. Lett.*, **5**, 025205, doi:10.1088/1748-9326/5/2/025205.

Allen, M., and W. Ingram, 2002: Constraints on future changes in climate and the hydrologic cycle. *Nature*, **419**, 224–232, doi:10.1038/nature01092.

Bengtsson, L., K. Hodges, and E. Roeckner, 2006: Storm tracks and climate change. *J. Climate*, **19**, 3518–3543, doi:10.1175/JCLI3815.1.

——, ——, S. Koumoutsaris, M. Zahn, and N. Keenlyside, 2011: The changing atmospheric water cycle in polar regions in a warmer climate. *Tellus*, **63A**, 907–920, doi:10.1111/j.1600-0870.2011.00534.x.

Bintanja, R., and F. Selten, 2014: Future increases in Arctic precipitation linked to local evaporation and sea-ice retreat. *Nature*, **509**, 479–482, doi:10.1038/nature13259.

Boer, G., 1993: Climate change and the regulation of the surface moisture and energy budgets. *Climate Dyn.*, **8**, 225–239, doi:10.1007/BF00198617.

Bosilovich, M., S. Schubert, and G. Walker, 2005: Global changes in water cycle intensity. *J. Climate*, **18**, 1591–1608, doi:10.1175/JCLI3357.1.

Chang, E., Y. Guo, and X. Xia, 2012: CMIP5 multimodel ensemble projection of storm track change under global warming. *J. Geophys. Res.*, **117**, D23118, doi:10.1029/2012JD018578.

Chou, C., J.-Y. Tu, and P.-H. Tan, 2007: Asymmetry of tropical precipitation change under global warming. *Geophys. Res. Lett.*, **34**, L17708, doi:10.1029/2007GL030327.

Dai, A., 2012: Increasing drought under global warming in observations and models. *Nat. Climate Change*, **3**, 52–58, doi:10.1038/nclimate1633.

Durack, P., S. Wijffels, and R. Matear, 2012: Ocean salinities reveal strong global water cycle intensification during 1950 to 2000. *Science*, **336**, 455–458, doi:10.1126/science.1212222.

Gimeno, L., R. Nieto, A. Drumond, R. Castillo, and R. Trigo, 2013: Influence of the intensification of the major oceanic moisture sources on continental precipitation. *Geophys. Res. Lett.*, **40**, 1443–1450, doi:10.1002/grl.50338.

Hall, N., B. Hoskins, P. Valdes, and C. Senior, 1994: Storm tracks in a high-resolution GCM with doubled carbon dioxide. *Quart. J. Roy. Meteor. Soc.*, **120**, 1209–1230, doi:10.1002/qj.49712051905.

Held, I., and B. Soden, 2006: Robust responses of the hydrological cycle to global warming. *J. Climate*, **19**, 5686–5699, doi:10.1175/JCLI3990.1.

Helm, K., N. Bindoff, and J. Church, 2010: Changes in the global hydrological-cycle inferred from ocean salinity. *Geophys. Res. Lett.*, **37**, L18701, doi:10.1029/2010GL044222.

Hu, P., T. Li, J.-J. Luo, H. Murakami, A. Kitoh, and M. Zhao, 2012: Increase of global monsoon area and precipitation under global warming: A robust signal? *Geophys. Res. Lett.*, **39**, L06701, doi:10.1029/2012GL051037.

Hwang, Y.-T., and D. Frierson, 2010: Increasing atmospheric poleward energy transport with global warming. *Geophys. Res. Lett.*, **37**, L24807, doi:10.1029/2010GL045440.

Kidston, J., S. Dean, J. Renwick, and G. Vallis, 2010: A robust increase in the eddy length scale in the simulation of future climates. *Geophys. Res. Lett.*, **37**, L03806, doi:10.1029/2009GL041615.

Lau, W., H.-T. Wu, and K.-M. Kim, 2013: A canonical response of precipitation characteristics to global warming from CMIP5 models. *Geophys. Res. Lett.*, **40**, 3163–3169, doi:10.1002/grl.50420.

Lorenz, D., 2014: Understanding midlatitude jet variability and change using Rossby wave chromatography: Poleward-shifted jets in response to external forcing. *J. Atmos. Sci.*, **71**, 2370–2389, doi:10.1175/JAS-D-13-0200.1.

——, E. DeWeaver, and D. Vimont, 2010: Evaporation change and global warming: The role of net radiation and relative humidity. *J. Geophys. Res.*, **115**, D20118, doi:10.1029/2010JD013949.

Manabe, S., and R. Wetherald, 1975: The effects of doubling the CO_2 concentration on the climate of a general circulation model. *J. Atmos. Sci.*, **32**, 3–15, doi:10.1175/1520-0469(1975)032<0003:TEODTC>2.0.CO;2.

Meehl, G., J. Arblaster, and C. Tebaldi, 2005: Understanding future patterns of increased precipitation intensity in climate model simulations. *Geophys. Res. Lett.*, **32**, L18719, doi:10.1029/2005GL023680.

Mitchell, J., C. Wilson, and W. Cunnington, 1987: On CO_2 climate sensitivity and model dependence of results. *Quart. J. Roy. Meteor. Soc.*, **113**, 293–322, doi:10.1002/qj.49711347517.

Muller, C., and P. O'Gorman, 2011: An energetic perspective on the regional response of precipitation to climate change. *Nat. Climate Change*, **1**, 266–271, doi:10.1038/nclimate1169.

O'Gorman, P., 2010: Understanding the varied response of the extratropical storm tracks to climate change. *Proc. Natl. Acad. Sci. USA*, **107**, 19 176–19 180, doi:10.1073/pnas.1011547107.

Peixoto, J., and A. Oort, 1992: *Physics of Climate.* American Institute of Physics, 520 pp.

Pendergrass, A., and D. Hartmann, 2014: The atmospheric energy constraint on global-mean precipitation change. *J. Climate*, **27**, 757–768, doi:10.1175/JCLI-D-13-00163.1.

Richter, I., and S. Xie, 2008: Muted precipitation in global warming simulations: A surface evaporation perspective. *J. Geophys. Res.*, **113**, D24118, doi:10.1029/2008JD010561.

Rivière, G., 2011: A dynamical interpretation of the poleward shift of the jet streams in global warming scenarios. *J. Atmos. Sci.*, **68**, 1253–1272, doi:10.1175/2011JAS3641.1.

Scheff, J., and D. Frierson, 2012a: Robust future precipitation declines in CMIP5 largely reflect the poleward expansion of model subtropical dry zones. *Geophys. Res. Lett.*, **39**, L18704, doi:10.1029/2012GL052910.

——, and ——, 2012b: Twenty-first-century multimodel subtropical precipitation declines are mostly midlatitude shifts. *J. Climate*, **25**, 4330–4347, doi:10.1175/JCLI-D-11-00393.1.

Seager, R., and Coauthors, 2007: Model projections of an imminent transition to a more arid climate in southwestern North America. *Science*, **316**, 1181–1184, doi:10.1126/science.1139601.

——, N. Naik, and G. Vecchi, 2010: Thermodynamic and dynamic mechanisms for large-scale changes in the hydrological cycle in response to global warming. *J. Climate*, **23**, 4651–4668, doi:10.1175/2010JCLI3655.1.

Seidel, D., Q. Fu, W. Randel, and T. Reichler, 2008: Widening of the tropical belt in a changing climate. *Nat. Geosci.*, **1**, 21–24, doi:10.1038/ngeo.2007.38.

Serreze, M., A. Barrett, and J. Stroeve, 2012: Recent changes in tropospheric water vapor over the Arctic as assessed from radiosondes and atmospheric reanalyses. *J. Geophys. Res.*, **117**, D10104, doi:10.1029/2011JD017421.

Sherwood, S., and Q. Fu, 2014: A drier future? *Science*, **343**, 737–739, doi:10.1126/science.1247620.

Singh, H., C. Bitz, J. Nusbaumer, and D. Noone, 2016a: A mathematical framework for analysis of water tracers: Part I: Development of theory and application to the preindustrial mean state. *J. Adv. Model. Earth Syst.*, **8**, 991–1013, doi:10.1002/2016MS000649.

——, A. Donohoe, C. Bitz, J. Nusbaumer, and D. Noone, 2016b: Greater aerial transport distances with warming amplify interbasin salinity contrasts. *Geophys. Res. Lett.*, doi:10.1002/2016gl069796, in press.

Stephens, G., and T. Ellis, 2008: Controls of global-mean precipitation increases in global warming GCM experiments. *J. Climate*, **21**, 6141–6155, doi:10.1175/2008JCLI2144.1.

——, A. Slingo, M. Webb, P. Minnett, P. Daum, L. Kleinman, I. Wittmeyer, and D. Randall, 1994: Observations of the earth's radiation budget in relation to atmospheric hydrology: 4. Atmospheric column radiative cooling over the world's oceans. *J. Geophys. Res.*, **99**, 18 585–18 604, doi:10.1029/94JD01151.

Trenberth, K., 1998: Atmospheric moisture residence times and cycling: Implications for rainfall rates and climate change. *Climatic Change*, **39**, 667–694, doi:10.1023/A:1005319109110.

Vallis, G., P. Zurita-Gotor, C. Cairns, and J. Kidston, 2014: Response of the large-scale structure of the atmosphere to global warming. *Quart. J. Roy. Meteor. Soc.*, **141**, 1479–1501, doi:10.1002/qj.2456.

van der Ent, R., and H. Savenije, 2011: Length and time scales of atmospheric moisture recycling. *Atmos. Chem. Phys.*, **11**, 1853–1863, doi:10.5194/acp-11-1853-2011.

Vecchi, G., and B. Soden, 2007: Global warming and the weakening of the tropical circulation. *J. Climate*, **20**, 4316–4340, doi:10.1175/JCLI4258.1.

Wegmann, M., and Coauthors, 2015: Arctic moisture source for Eurasian snow cover variations in autumn. *Environ. Res. Lett.*, **10**, 054015, doi:10.1088/1748-9326/10/5/054015.

Willett, K., N. Gillett, P. Jones, and P. Thorne, 2007: Attribution of observed surface humidity changes to human influence. *Nature*, **449**, 710–712, doi:10.1038/nature06207.

Yin, J., 2005: A consistent poleward shift of the storm tracks in simulations of 21st century climate. *Geophys. Res. Lett.*, **32**, L18701, doi:10.1029/2005GL023684.

Zhang, X., F. Zwiers, G. Hegerl, F. Lambert, N. Gillett, S. Solomon, P. Stott, and T. Nozawa, 2007: Detection of human influence on twentieth-century precipitation trends. *Nature*, **448**, 461–465, doi:10.1038/nature06025.